



Rate limiting steps of the porous $\text{La}_{0.6}\text{Sr}_{0.4}\text{Co}_{0.8}\text{Fe}_{0.2}\text{O}_{3-\delta}$ electrode material

N. Grunbaum^{a,b}, L. Dessemond^a, J. Fouletier^a, F. Prado^b, L. Mogni^{b,c}, A. Caneiro^{b,c,*}

^a Laboratoire d'Electrochimie et de Physicochimie des Matériaux et des Interfaces (L.E.P.M.I.), E.N.S.E.E.G., I.N.P. Grenoble, BP 75 38402 Saint Martin D'Heres Cedex, France

^b Centro Atómico Bariloche, CNEA, 8400 S.C. de Bariloche RN, Argentina

^c CONICET (Consejo Nacional de Investigaciones Científicas y Técnicas) Argentina

ARTICLE INFO

Article history:

Received 9 June 2008

Received in revised form 4 September 2009

Accepted 11 September 2009

Keywords:

Mixed conductors

Electrode reaction

Cobaltites

SOFC

Impedance spectroscopy

ABSTRACT

The electrode reaction of porous $\text{La}_{0.6}\text{Sr}_{0.4}\text{Co}_{0.8}\text{Fe}_{0.2}\text{O}_{3-\delta}$ films deposited onto $\text{Ce}_{0.9}\text{Gd}_{0.1}\text{O}_{1.95}$ (CGO) was investigated by impedance spectroscopy within the temperature and oxygen partial pressure ($p\text{O}_2$) ranges of $500 \leq T \leq 700$ °C and $10^{-4} < p\text{O}_2 < 1$ atm, respectively, using Ar and He as gas carriers. The electrochemical impedance spectroscopy (EIS) measurements reveal a high frequency (HF) and a low frequency (LF) regions in the Nyquist plane. The high frequency (HF) region was fitted with a Warburg-type impedance element, and the low frequency (LF) region was reproduced with a resistance in parallel to a constant phase element. Both, the slight dependence of the polarization resistance (R_{W}) and the small variation of the apex frequency (f_{v}) of the HF Warburg-type element, on $p\text{O}_2$, suggest that this contribution corresponds to the oxygen diffusion in the bulk of the $\text{La}_{0.6}\text{Sr}_{0.4}\text{Co}_{0.8}\text{Fe}_{0.2}\text{O}_{3-\delta}$ electrode material. The variation of the polarization resistance of the LF region (R_{rcpe}) with $p\text{O}_2$ indicates that as T increases, the limiting step evolves from dissociative oxygen adsorption to oxygen gas diffusion in the pores of the mixed ionic/electronic conductor (MIEC) electrode.

© 2009 Elsevier B.V. All rights reserved.

1. Introduction

Transition metal oxides of general formula $\text{La}_{1-x}\text{Sr}_x\text{Co}_{1-y}\text{Fe}_y\text{O}_{3-\delta}$ (LSCF) with perovskite structure have been extensively investigated as cathode in solid oxide fuel cells (SOFC) because they exhibit non negligible oxide-ion conductivity (σ_i) together with high electronic conductivity (σ_e) [1,2]. The ionic conductivity of these mixed ionic/electronic conductors (MIECs) improves with increasing Sr and Co content. However, compounds with large Sr content exhibit an order/disorder transition [3,4], which is suppressed by partial substitution of Sr^{2+} by La^{3+} [5]. Ionic conduction in LSCF materials yields an extension of the electrochemical active zone beyond the triple phase boundary (TPB) consequently reducing the polarization resistance to lower values than those of electronic conductors such as Pt or $(\text{La,Sr})\text{MnO}_3$ manganites [6–11]. In addition, LSCF compounds with high Co content show good catalytic activity to the oxygen reduction at intermediate temperatures [12] and chemical compatibility with gadolinia-doped ceria (CGO) [13,14]. Thus, $\text{La}_{1-x}\text{Sr}_x\text{Co}_{1-y}\text{Fe}_y\text{O}_{3-\delta}$ perovskites with $0.2 \leq x \leq 0.6$ and $0 \leq y \leq 0.2$ are considered suitable cathode materials for intermediate temperatures SOFC (IT-SOFC) using either YSZ [15–17] or CGO [18–21] electrolytes.

The overall oxygen reduction mechanism at the cathode involves several processes such as gas phase diffusion in the pores of the electrode, oxygen exchange at the gas/electrode interface (adsorp-

tion, charge transfer, etc.), diffusion of oxygen ions through the electrode material and the transfer of oxygen ions at the electrode/electrolyte interface.

Different mechanisms have been proposed and discussed regarding oxygen reduction in the literature, based on either experimental data or computational modeling [6,7,17–19,21–24]. However, the understanding of the oxygen reduction reaction at the cathode material is still poor because of the influence of a large number of variables such as electronic and ionic conductivities, microstructure, temperature, atmosphere, polarization, and the occurrence of coupled processes. For Co rich LSCF perovskites, oxygen reduction has been investigated on dense [17,24,25] and porous [16,18,19,21] electrodes deposited on YSZ [16,17,24] or CGO [18,19,21,25]. While the contribution of the transfer of oxygen ions at the electrode/electrolyte interface has been clearly observed for dense LSC electrodes on YSZ [24], oxygen diffusion in the gas phase and in the bulk of the electrode material is the most common limiting step for porous MIEC electrodes [8,19,21,25].

This type of studies can be performed using electrochemical cells with either two or three electrodes. The three electrodes cell allows the application of a dc bias and, therefore the study of the electrode reaction under either cathodic or anodic polarization. For example, far from equilibrium phenomena can be triggered such as the creation of oxygen vacancies in LSM electrodes under moderate cathodic polarization [10,11]. Studies with dc bias can also be performed making use of a cell with two electrodes built with microelectrodes and extended counter-electrode [26,27]. The two electrodes symmetrical cell is a simple configuration used for studying the electrode

* Corresponding author. Tel.: +54 2944445274; fax: +54 2944445299.
E-mail address: caneiro@cab.cnea.gov.ar (A. Caneiro).

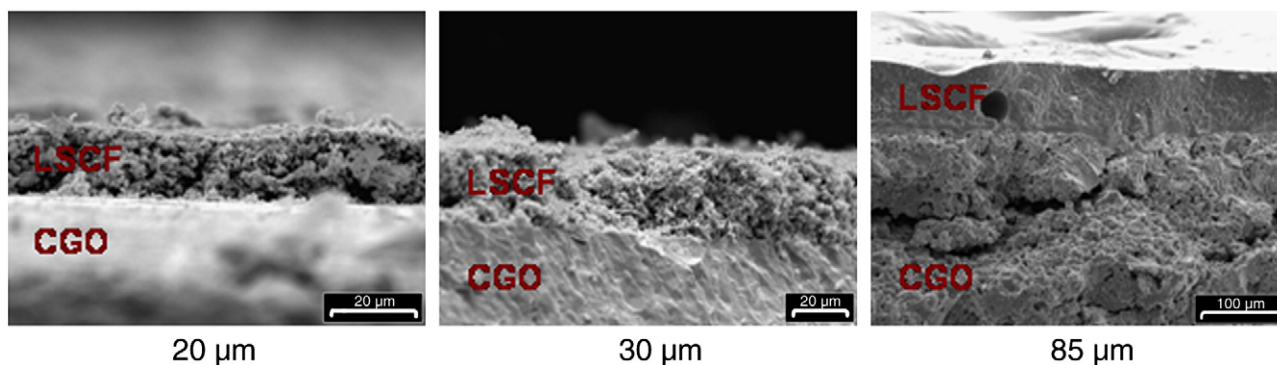


Fig. 1. SEM micrographs of the cross-section of the $\text{La}_{0.6}\text{Sr}_{0.4}\text{Co}_{0.8}\text{Fe}_{0.2}\text{O}_{3-\delta}$ films deposited on CGO.

reaction around a steady state under zero polarization. The use of atmospheres with controlled $p\text{O}_2$ permits the identification of the limiting steps of the electrode reaction from the relationship between the polarization resistance and $p\text{O}_2$ [11]. The aim of the present work was to perform a detailed study of the electrode reaction of the porous $\text{La}_{0.6}\text{Sr}_{0.4}\text{Co}_{0.8}\text{Fe}_{0.2}\text{O}_{3-\delta}$ onto $\text{Ce}_{0.9}\text{Gd}_{0.1}\text{O}_{1.95}$ making use of a symmetrical cell coupled to an accurate electrochemical gas blending system [28]. We selected the $\text{La}_{0.6}\text{Sr}_{0.4}\text{Co}_{0.8}\text{Fe}_{0.2}\text{O}_{3-\delta}$ composition taking into account the low polarization resistance exhibited by this material [21].

The EIS measurements revealed the presence of a high frequency contribution (HF) and a low frequency (LF) one. The high frequency response was fitted with a Warburg-type element associated to the diffusion of oxygen ions in the bulk of the electrode. The low frequency contribution was assigned to dissociative oxygen adsorption at lower temperatures and to oxygen gas diffusion in the pores of the MIEC electrode at higher temperatures.

2. Experimental

$\text{La}_{0.6}\text{Sr}_{0.4}\text{Co}_{0.8}\text{Fe}_{0.2}\text{O}_{3-\delta}$ (LSCF) samples were prepared by an acetic acid based gel route [29] using SrCO_3 , La_2O_3 , $\text{Fe}(\text{CH}_3\text{COO})_2 \cdot 1.38\text{H}_2\text{O}$ and $\text{Co}(\text{CH}_3\text{COO})_2 \cdot 4\text{H}_2\text{O}$ as starting materials. Stoichiometric amounts were weighed and dissolved in acetic acid. The mixture was refluxed at $T \sim 80^\circ\text{C}$ with the addition of water and small amounts of hydrogen peroxide until a clear solution was obtained. The solvents were evaporated on a hot plate to form a red transparent gel. This gel was then decomposed at 400°C for 30 min. The resulting powder was finally heated at 900°C for 6 h.

Dense pellets of $\text{Ce}_{0.9}\text{Gd}_{0.1}\text{O}_{1.95}$ (CGO) of approximately 11 mm in diameter and 1 mm thick were obtained by uniaxially pressing commercial CGO powder (PRAXAIR) and sintering at 1400°C for 6 h in air. The ink for electrode deposition was prepared by mixing the LSCF powders with ethanol, α -terpineol, polyvinyl butyral, and polyvinylpyrrolidone in 40:30:27:2:1 ratio. The electrochemical cell was prepared with the symmetrical configuration. Thick films were deposited by spraying the cathode ink onto both sides of the polished CGO substrate. Afterwards, these assemblies were heat treated at 1000°C for 1 h in air to promote a sufficient adherence between electrodes and electrolyte. The electrode thickness was controlled by the number of sprayed layers deposited onto the electrolyte.

The electrode thickness and morphology were determined by scanning electron microscopy (SEM) by using a Philips 515 microscope. Electrochemical impedance spectroscopy (EIS) measurements were performed under zero dc polarization by using a potentiostat/impedance analyzer Autolab (Echochemie BV) between 10^{-3} and 10^4 Hz, at different temperatures (500 , 600 and 700°C) and varying $p\text{O}_2$ between 3×10^{-4} and 1 atm. An ac signal of amplitude equal to 50 mV was applied to the cell with respect to the linearity of the electrical response. Platinum grids, slightly pressed on porous

electrodes, were used as current collectors. Impedance diagrams were resolved by using the EQUIVCRT software [30]. The $p\text{O}_2$ was controlled by means of an electrochemical pump and measured with an oxygen gauge [28]. The gas flow rate was fixed equal to 6 l/h. In order to study the influence of the gas phase on the recorded electrode characteristics, Ar and He were chosen as the carrier gases, based on the fact that O_2 diffusivity is higher in a He- O_2 mixture.

The formation of the LSCF perovskite phase was verified by X-ray diffraction ($10 \leq 2\theta \leq 70^\circ$) by using a Philips PW 1700 diffractometer with the Cu-K_α radiation and a graphite monochromator.

3. Results and discussion

Fig. 1 shows SEM micrographs of the cross-section of the $\text{La}_{0.6}\text{Sr}_{0.4}\text{Co}_{0.8}\text{Fe}_{0.2}\text{O}_{3-\delta}$ films on CGO after impedance measurements. Regardless of the electrode thickness, a good adhesion between both components was achieved. The electrode thicknesses (ℓ) determined from SEM observations were 20, 30 and 85 μm , respectively.

Taking into account that the sprayed electrodes were deposited by using the same ink and identical heating procedure for all investigated cells, all samples exhibit a similar morphology. A micrograph of the upper view of one $\text{La}_{0.6}\text{Sr}_{0.4}\text{Co}_{0.8}\text{Fe}_{0.2}\text{O}_{3-\delta}$ thick film is shown in Fig. 2. All studied samples are porous and LSCF grains are submicronic. Thus, porosity and tortuosity are assumed similar and the main varying microstructural parameter is the electrode thickness.

The XRD diffractograms obtained before and after the EIS measurements were practically identical with diffraction peaks corresponding to those of LSCF and CGO phases. No extra peaks due to secondary phases were detected. We also verified that no appreciable evolution of the impedance spectrum occurred, in spite of the long time period of our EIS measurements. These observations indicate that no reactivity took place between CGO and LSCF.

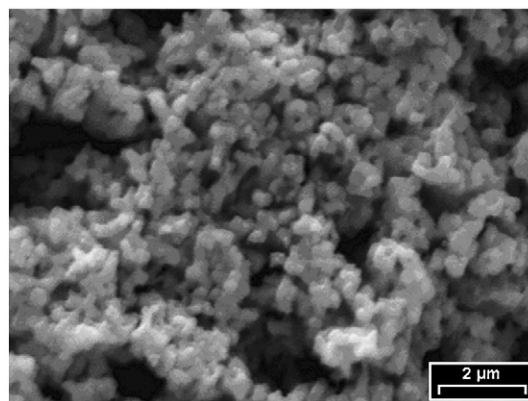


Fig. 2. Upper view of a $\text{La}_{0.6}\text{Sr}_{0.4}\text{Co}_{0.8}\text{Fe}_{0.2}\text{O}_{3-\delta}$ thick film ($\ell = 20 \mu\text{m}$).

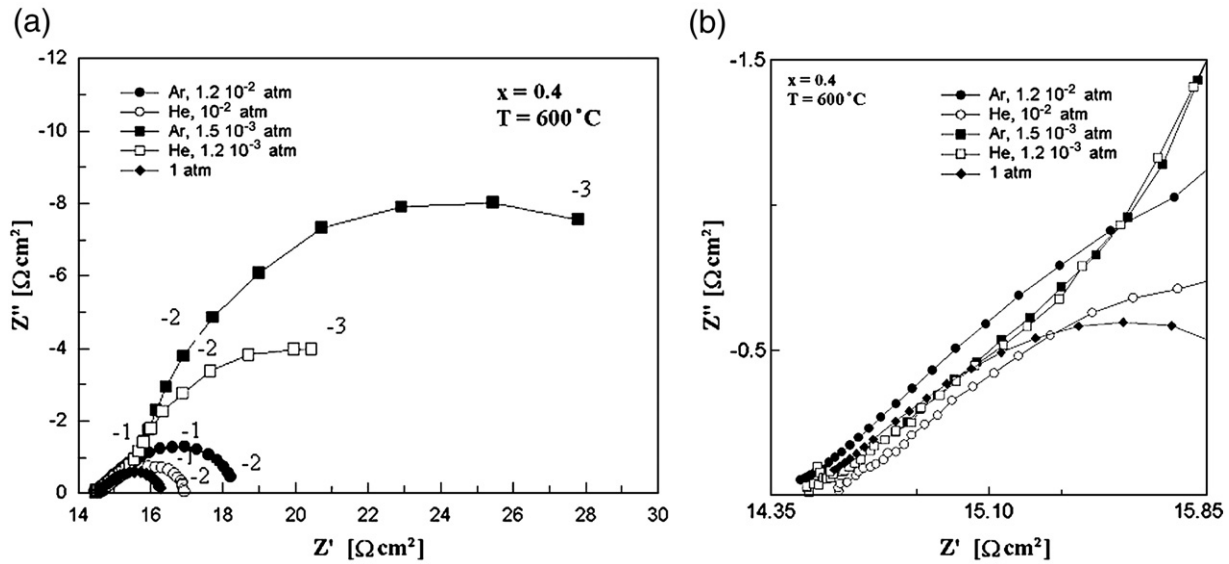


Fig. 3. (a) Impedance diagrams recorded at 600 °C ($\ell = 20 \mu\text{m}$) for different $p\text{O}_2$ and gas carriers. (b) High frequency parts of the electrode characteristics. The numbers indicate the logarithm of the measuring frequency.

Impedance diagrams recorded at 600 °C in different gas atmospheres for the 20 μm thick electrode are given in Fig. 3(a) and (b). The total polarization resistance R_{pol} , defined by the difference between the intersections of the low and high frequency limits of the electrode impedance with the real axis in the Nyquist plane, depends on $p\text{O}_2$, but also varies with the gas carrier. As $p\text{O}_2$ decreases, R_{pol} increases since the activity of the electroactive species like O_2 decreases. Thus, for example, mass control transfer mechanisms begin to be active. This effect is observed in the low frequency range. Another interesting result concerns the high frequency part of the recorded electrode impedance. As can be seen in Fig. 3b, all responses almost coincide indicating that the shape of the corresponding contribution does not depend on the gas atmosphere within the experimental accuracy. This result suggests that the electrolyte resistance, determined from the intersection of the high frequency limit of the electrode impedance with the real axis in the Nyquist plane, remains unchanged under the chosen experimental conditions. The 45° straight line observed at high frequencies is similar in shape to the well known finite-length Warburg impedance. Thus, this contribution could be related to a diffusion process of oxygen ions through the electrode material [21,24,31]. The occurrence of such a high frequency contribution in the impedance response of a LSM-YSZ composite electrode has been already ascribed to ionic transport through YSZ [32].

Under pure oxygen, at the equilibrium, no oxygen concentration gradient in the porous electrode is expected [33] and the contribution of gaseous diffusion can be neglected. The impedance diagram recorded under these experimental conditions was fitted either with a Gerischer-type or a Warburg-type element. The former element is dedicated to the response of a porous electrode while the latter describes a dense electrode material [18,19]. Nevertheless, the higher accuracy on fitting experimental data was obtained with a Warburg-type impedance described by the following expression [34]:

$$Z_{\text{W}}(\omega) = \frac{RT}{4F^2} \frac{1}{SC_{\text{v}}} \frac{th(l\sqrt{j\omega}/D_{\text{v}})}{\sqrt{j\omega}D_{\text{v}}} \quad (1)$$

where R and F are the ideal gas and Faraday constants, S is the electrode/electrolyte interface area, C_{v} is the oxygen vacancy concentration at the electrode/electrolyte interface, D_{v} is the vacancy diffusion coefficient and ω is the measuring angular frequency.

In case of a dense electrode, the parameter l is determined by the electrode thickness. In this study, this parameter is likely to correspond to an effective length wherein the electrode is electrochemically active, which is much lower than the porous electrode thickness (ℓ) [8,18,19]. The corresponding polarization resistance (R_{w}) is given by:

$$R_{\text{w}} = \frac{RT}{4F^2} \frac{1}{SC_{\text{v}}} \frac{l}{D_{\text{v}}} \quad (2)$$

According to the behavior depicted in Fig. 3, the HF contribution was always fitted with a Warburg-type impedance regardless of the value of the oxygen partial pressure. Thus, the electrode impedances were analyzed by means of an electrical equivalent circuit which consists of a pure resistive element R_{elec} representing the electrolyte resistance connected in series with a high frequency (HF) finite-length Warburg impedance (W) and a circuit element consisting of a resistance in parallel with a constant phase element (Fig. 4). This last combination is used to fit the low frequency (LF) range of the impedance diagram which is highly sensitive to the oxygen partial pressure. The resistances corresponding to both contributions are referenced as R_{w} and R_{rcpe} , respectively.

Within the experimental error, R_{w} is an increasing function of $p\text{O}_2$ and does not depend on the gas carrier (Fig. 5a). This further confirms that the high frequency contribution cannot be related to any process involving gaseous species. On the other hand, according to Eq. (2) and assuming that the oxygen diffusion coefficient remains unchanged within the $p\text{O}_2$ range used in this study, the variation of R_{w} with $p\text{O}_2$ seems to be related mainly to the variation of the oxygen vacancy concentration, C_{v} , with $p\text{O}_2$. This result was confirmed through independent thermodynamic measurements of the equilibrium $p\text{O}_2$ as a function of the oxygen content for $\text{La}_{0.6}\text{Sr}_{0.4}\text{Co}_{0.8}\text{Fe}_{0.2}\text{O}_{3-\delta}$ at

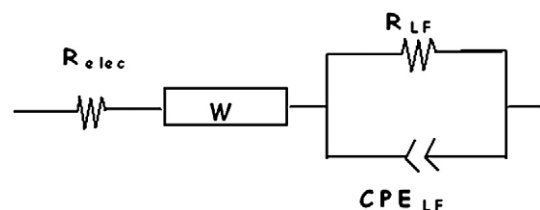


Fig. 4. Equivalent circuit of the experimental impedances.

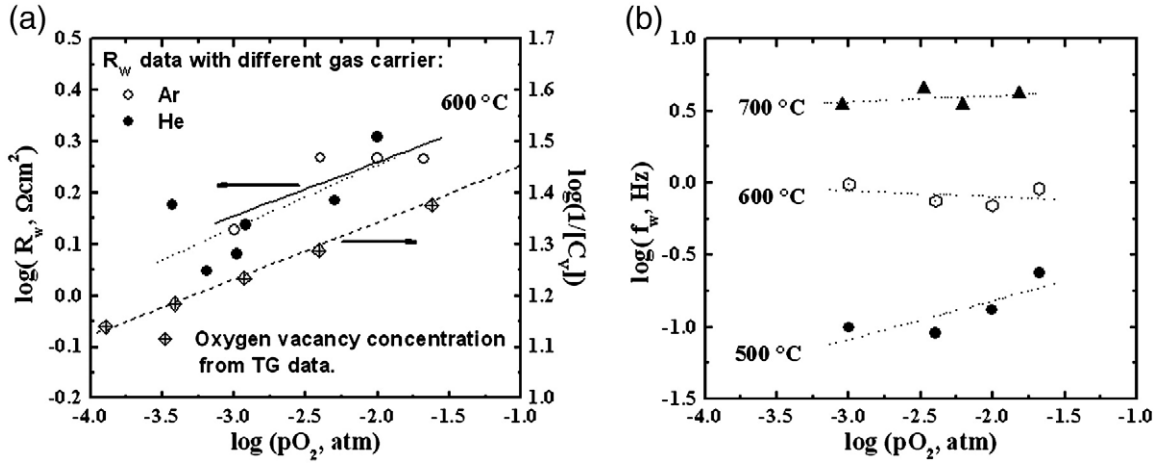


Fig. 5. (a): Variations of R_w and $1/[C_v]$ vs. pO_2 at 600 °C using He and Ar as gas carriers. (b): Variation of the apex frequency of the Warburg-type impedance “ f_w ” vs. pO_2 at 500, 600 and 700 °C.

$T = 500$ °C. Further details about this type of measurements are given in [4,5]. In Fig. 5a can be observed that the $\log(R_w)$ vs. $\log(pO_2)$ curve has the same slope as the $\log(1/[C_v])$ vs. $\log(pO_2)$ curve, clearly indicating that the main variable affecting R_w is the oxygen vacancy concentration C_v . Thus, lower values of pO_2 lead to an increase of the oxygen vacancy concentration and therefore to higher ionic conductivity values and lower associated polarization resistance for the electrode material [35].

Useful information can also be extracted from the apex frequency of the Warburg-type element (corresponding to the minimum of the imaginary part of the measured impedance in the Nyquist plane). As shown in Fig. 5b, the apex frequency is nearly independent of the pO_2 . This result confirms that the observed process is not mixed controlled and can be thus related only to the diffusion of oxygen ions through the LSCF electrode [7].

The LF resistance (R_{rpe}) exhibits a stronger dependence with the pO_2 , whatever the measuring temperature (Fig. 6). In general, the experimental data can be fitted with a power law as follows:

$$R_{rpe} = C \times (P_{O_2})^n \quad (3)$$

where C is a constant and n an exponent that depends on the kinetic limiting step [11,15,24]. If $n = -1$, the limiting processes can be oxygen diffusion in the gas phase or molecular adsorption on the surface of the electrode and a value of -0.5 corresponds to a dissociative adsorption of oxygen. In a porous electrode material, the

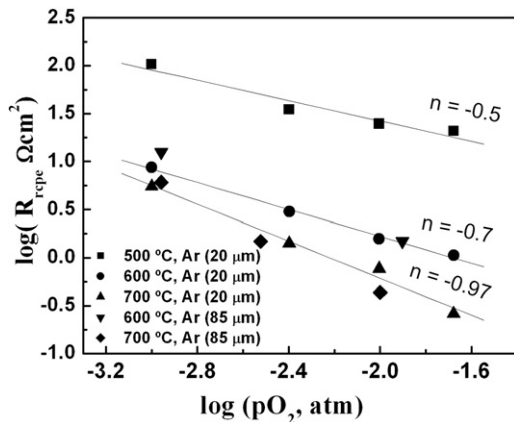


Fig. 6. Variation of R_{rpe} vs. pO_2 at different temperatures for different thicknesses (gas carrier: Ar).

polarization resistance due to O_2 diffusion in the gas phase can be expressed by [34]:

$$R_{diff} = 2 \frac{RT}{(4F)^2} \frac{L}{D_{O_2}^{eff}} (pO_2)^{-1} \quad (4)$$

where L is the length of the pore and $D_{O_2}^{eff}$ is the effective diffusion coefficient for molecular oxygen.

Gas phase diffusion in porous electrodes can proceed by different mechanisms. When interactions between diffusing molecules and the pore walls are negligible ($\lambda \ll d$, where λ is the average free length of the O_2 molecule and d is the pore diameter), normal gas bulk diffusion predominates. On the other hand, Knudsen diffusion is the main mechanism when collisions of the molecules with the pore walls control the diffusion process ($\lambda \gg d$). Since the average pore size of investigated electrodes is of the order of $1 \mu\text{m}$ (Fig. 2), both mechanisms were considered. The resulting effective diffusion coefficient involves contributions of bulk and Knudsen processes according to [36]:

$$\frac{1}{D_{O_2}^{eff}} = \frac{1}{D_{O_2}^k} + \frac{L}{D_{O_2}^b} \quad (5)$$

where $D_{O_2}^k$ and $D_{O_2}^b$ represent the diffusion coefficient related to both processes.

By assuming a dissociative oxygen adsorption, the corresponding polarization resistance is [16,24,36]:

$$R_{ads} = \frac{RT}{(2F)^2} \frac{1}{k} (pO_2)^{-1/2} \quad (6)$$

where k represents the rate constant for oxygen adsorption.

The first obvious result is that n depends on the measuring temperature (see Fig. 6). At 700 °C, the experimental data was fitted using a $n = -1$ value in Eq. (6), while at $T = 500$ °C the best fit was obtained using $n = -0.5$. The exponent value was found equal to -0.7 for measurements performed at 600 °C. The variation of n with the measuring temperature suggests a modification of the kinetic limiting LF process. By increasing temperature, the limiting step evolves from dissociative adsorption of oxygen to oxygen diffusion in the gas phase of the porous electrode. It is worth mentioning that such an evolution is not surprising since pore polarization is generally evidenced at high temperatures [33]. Both processes (adsorption and gas phase diffusion) have polarizations resistances with a thermal activated behavior. Since the oxygen adsorption is related to the k constant and oxygen gas diffusion to $D_{O_2}^{eff}$, the evolution of the

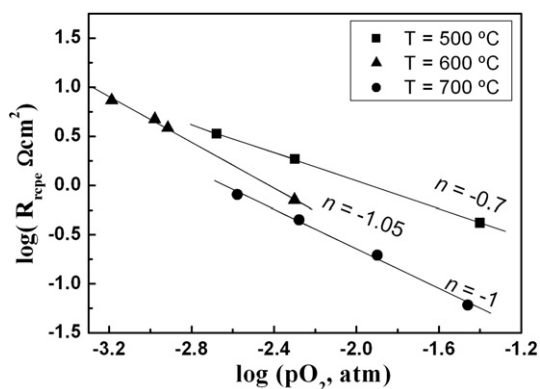


Fig. 7. Variation of R_{rcpe} vs. pO_2 at different temperatures (gas carrier: He).

limiting step with T suggests that the activation energy for diffusion is lower than that of adsorption. Then, the pore diffusion is the dominating process at high temperatures. Finally, at 600 °C, the value of n can be related to a mixed kinetic control of the low frequency process involving adsorption of oxygen and gas phase diffusion.

The results shown in Fig. 6 also underline that R_{rcpe} does not depend on the electrode thickness, whereas as it was reported R_W increases with this parameter [21]. This clearly proves that the low frequency process can be related to an interfacial process, at least at the lowest temperatures. This is in agreement with a theoretical analysis of a gas diffusion process in porous electrodes predicting that an increase of the electrode thickness of 100 μm would result in an increase of the electrode overpotential of less than 1–3 mV [37]. Therefore, R_{rcpe} is not sensitive to the electrode thickness.

Regardless of the measuring temperature, the magnitude of the low frequency process decreases when He is used instead of Ar as gas carrier (Fig. 7). At 700 °C, a first power pO_2 dependency for R_{rcpe} was recorded, in a perfect agreement with measurements performed in the Ar– O_2 mixture (Fig. 6). This result further suggests that the low frequency rate limiting step is gas diffusion at high temperature. The diminution of the polarization resistance is caused by the higher effective O_2 diffusivity in the He– O_2 mixture than in the Ar– O_2 one (Eq. (4)). Below 700 °C, for a given temperature, the value of n in Eq. (3) is higher when He is used as gas carrier. If one refers to Eq. (6), one could still expect an exponent equal to -0.5 if the adsorption process is the rate determining step at low temperatures, by assuming that the rate constant does not depend on the gas carrier. At this stage, the obtained results suggest that adsorption is likely to be enhanced in the He– O_2 mixture, and thus a mixed kinetic control of the low frequency process is observed at lower temperatures than in the Ar– O_2 mixture. The higher n value determined at 600 °C is in agreement with this assumption. The origin of this enhancement remains still unclear.

4. Conclusions

The electrode reaction of porous $\text{La}_{0.6}\text{Sr}_{0.4}\text{Co}_{0.8}\text{Fe}_{0.2}\text{O}_{3-\delta}$ thick films deposited on dense $\text{Ce}_{0.9}\text{Gd}_{0.1}\text{O}_{1.95}$ (CGO) pellets was investigated in detail by complex impedance spectroscopy within the temperature range, $500 \leq T \leq 700$ °C, making use of gas mixtures of controlled oxygen activity, $10^{-4} < pO_2 < 1$ atm., and Ar and He as gas carriers.

The use of these gas mixtures allowed us to separate in the Nyquist plane a HF contribution practically not sensitive to the gas phase and a LF contribution strongly dependent with pO_2 and the gas carrier.

The HF region was fitted with a Warburg-type element and the LF one with a circuit element consisting of a resistance in parallel with a constant phase element.

The slight variation of the polarization resistance of the HF region (R_W) with pO_2 showing a $1/C_V$ dependence, and the small variation of the apex frequency (f_v) with pO_2 strongly suggest that this contribution corresponds to the oxygen diffusion in the bulk of the $\text{La}_{0.6}\text{Sr}_{0.4}\text{Co}_{0.8}\text{Fe}_{0.2}\text{O}_{3-\delta}$ material.

The fitting of the polarization resistance of the LF region with a $R_{rcpe} = C \times (pO_2)^n$ law suggests that the limiting step evolves from dissociative oxygen adsorption to oxygen gas diffusion in the pores of the MIEC electrode as the temperature increases. The evolution from oxygen adsorption to gas diffusion depends on the gas carrier. This fact suggests that the rate constant for adsorption is higher for He as gas carrier.

Acknowledgements

This work was supported by CNEA (Argentine Atomic Energy Commission), ANPCyT (PICT 03-12-12455, 2006-00829 and 2007-02288), CONICET (PIP 5594), French-Argentine ECOS-SUD Cooperation Program (Project A02E02) and UNCuyo (Project 06/C183 and 06/C237).

References

- [1] S.J. Skinner, *Int. J. Inorg. Mater.* 3 (2001) 113.
- [2] H.J. Bouwmeester, A.J. Burggraf, in: P.E. Gellings, H.J. Bouwmeester (Eds.), *The CRC Handbook of Solid State Electrochemistry*, CRC Press, Boca Raton, FL, 1997, Chapter 14.
- [3] L.M. Liu, T.H. Lee, L. Qiu, Y.L. Yang, A.J. Jacobson, *Mater. Res. Bull.* 31 (1996) 29.
- [4] N. Grunbaum, L. Mogni, F. Prado, A. Caneiro, *J. Solid State Chem.* 177 (2004) 2350.
- [5] F. Prado, N. Grunbaum, A. Caneiro, A. Manthiram, *Solid State Ionics* 167 (2004) 147.
- [6] M. Liu, *J. Electrochem. Soc.* 145 (1998) 142.
- [7] J. Deseure, Y. Bultel, L. Dessemond, E. Siebert, *Solid State Ionics* 176 (2005) 235.
- [8] M. Koyama, C.J. Weng, T. Masuyama, J. Otomo, H. Fukinaga, K. Yamada, K. Egushi, H. Takahashi, *J. Electrochem. Soc.* 148 (2001) A795.
- [9] F.H. van Heuvelen, H.J.M. Bouwmeester, *J. Electrochem. Soc.* 144 (1997) 134.
- [10] A. Hammouche, F. Siebert, A. Hammou, M. Kleitz, A. Caneiro, *J. Electrochem. Soc.* 138 (1991) 1212.
- [11] E. Siebert, A. Hammouche, M. Kleitz, *Electrochim. Acta* 40 (1995) 1753.
- [12] Y. Matsumoto, S. Yamada, T. Nishida, E. Sato, *J. Electrochem. Soc.* 127 (1999) 2360.
- [13] A. Tsoga, A. Gupta, A. Naoumidis, P. Nikolopoulos, *Acta Mater.* 48 (2000) 4709.
- [14] G.C. Kostoglouidis, C. Ftikos, *Solid State Ionics* 126 (1999) 143.
- [15] Y. Takeda, R. Kanno, M. Noda, Y. Tomoda, O. Yamamoto, *J. Electrochem. Soc.* 134 (1987) 2656.
- [16] D.Z. de Florio, R. Muccillo, V. Esposito, E. Di Bartolomeo, E. Traversa, *J. Electrochem. Soc.* 152 (2005) A88.
- [17] F. Baumann, J. Fleig, H.U. Habermeier, J. Maier, *Solid State Ionics* 177 (2006) 1071–1081.
- [18] S.B. Adler, J.A. Lane, B.C.H. Steele, *J. Electrochem. Soc.* 143 (1996) 3554.
- [19] S.B. Adler, *Solid State Ionics* 111 (1998) 125.
- [20] J.M. Ralph, A.C. Schoeller, M. Krumpelt, *J. Mater. Sci.* 36 (2001) 1161.
- [21] N. Grunbaum, L. Dessemond, J. Fouletier, F. Prado, A. Caneiro, *Solid State Ionics* 177 (2006) 907.
- [22] S.B. Adler, *Chem. Rev.* 104 (2004) 4791.
- [23] J. Jamnik, J. Maier, *Phys. Chem. Chem. Phys.* 3 (2001) 1668.
- [24] A. Ringuedé, J. Fouletier, *Solid State Ionics* 139 (2001) 167.
- [25] V. Dusastre, J.A. Kilner, *Solid State Ionics* 126 (1999) 163.
- [26] F.S. Baumann, J. Fleig, H.-U. Habermeier, J. Maier, *Solid State Ionics* 177 (2006) 1071.
- [27] F.S. Baumann, J. Maier, J. Fleig, *Solid State Ionics* 179 (2008) 1198.
- [28] A. Caneiro, M. Bonnat, J. Fouletier, *J. Appl. Electrochem.* 11 (1981) 83.
- [29] Y. Xia, T. Armstrong, F. Prado, A. Manthiram, *Solid State Ionics* 130 (2000) 81.
- [30] B.A. Boukamp, *Solid State Ionics* 20 (1986) 31.
- [31] A. Ringuedé, J. Guindet, *Ionics* 3 (1997) 256.
- [32] M.J. Jorgensen, S. Primdhal, C. Bagger, M. Mogensen, *Solid State Ionics* 139 (2001) 1.
- [33] K. Huang, *J. Electrochem. Soc.* 151 (2004) H117.
- [34] I.D. Raistrick, J.R. Macdonald, D.R. Franceschetti, *Impedance Spectroscopy*, in: J.R. Macdonald (Ed.), *Emphasizing Solid Materials and Systems*, John Wiley and Sons, New York, 1987, Chapter 2.
- [35] J. Deseure, Y. Bultel, L. Dessemond, E. Siebert, P. Ozil, *J. Appl. Electrochem.* 37 (2006) 129.
- [36] S.P. Yoon, S.W. Nam, J. Han, T.-H. Lim, S.-A. Hong, S.-H. Hyun, *Solid State Ionics* 166 (2004) 1.
- [37] K. Huang, *J. Electrochem. Soc.* 151 (2004) A716.